Broadband THz reflective polarization rotator by multiple plasmon resonances

Xiewen Wen[1,*] and Junrong Zheng[1,2]

[1]*Rice University, Department of Chemistry, MS 60, Houston, Texas 77005, USA*
[2] *junrong@rice.edu*
**xiewen.wen@rice.edu*

Abstract: We demonstrate a metamaterials-based THz broadband polarization rotator which is able to rotate linearly polarized THz wave by 90 degree within a wide frequency range (0.44 to 0.76 THz). The device is characterized both theoretically and experimentally. Analyses show that the multiple-plasmon-resonance is the key for the broadband feature and the phase-shift difference of the two reflection components is critical for the polarization conversion. The approach demonstrated in the work can be useful for constructing building blocks for THz polarimetry.

OCIS codes: (160.3918) Metamaterials; (250.5403) Plasmonics; (300.6495) Spectroscopy, terahertz.

References and links

1. L. Thrane, R. H. Jacobsen, P. Uhd Jepsen, and S. Keiding, "THz reflection spectroscopy of liquid water," Chem. Phys. Lett. **240**(4), 330–333 (1995).
2. K. Liu, M. Brown, and R. Saykally, "Terahertz laser vibration-rotation tunneling spectroscopy and dipole moment of a cage form of the water hexamer," J. Phys. Chem. A **101**(48), 8995–9010 (1997).
3. F. Maiwald, F. Lewen, V. Ahrens, M. Beaky, R. Gendriesch, A. Koroliev, A. Negirev, D. Paveljev, B. Vowinkel, and G. Winnewisser, "Pure rotational spectrum of HCN in the terahertz region: use of a new planar Schottky diode multiplier," J. Mol. Spectrosc. **202**(1), 166–168 (2000).
4. M. C. Beard, G. M. Turner, and C. A. Schmuttenmaer, "Terahertz spectroscopy," J. Phys. Chem. B **106**(29), 7146–7159 (2002).
5. N. Vieweg, B. M. Fischer, M. Reuter, P. Kula, R. Dabrowski, M. A. Celik, G. Frenking, M. Koch, and P. U. Jepsen, "Ultrabroadband terahertz spectroscopy of a liquid crystal," Opt. Express **20**(27), 28249–28256 (2012).
6. B. B. Hu and M. C. Nuss, "Imaging with terahertz waves," Opt. Lett. **20**(16), 1716–1718 (1995).
7. D. Mittleman, M. Gupta, R. Neelamani, R. Baraniuk, J. Rudd, and M. Koch, "Recent advances in terahertz imaging," Appl. Phys. B **68**(6), 1085–1094 (1999).
8. R. Köhler, A. Tredicucci, F. Beltram, H. E. Beere, E. H. Linfield, A. G. Davies, D. A. Ritchie, R. C. Iotti, and F. Rossi, "Terahertz semiconductor-heterostructure laser," Nature **417**(6885), 156–159 (2002).
9. J. F. O'Hara, R. Singh, I. Brener, E. Smirnova, J. Han, A. J. Taylor, and W. Zhang, "Thin-film sensing with planar terahertz metamaterials: sensitivity and limitations," Opt. Express **16**(3), 1786–1795 (2008).
10. D. R. Smith, J. B. Pendry, and M. C. Wiltshire, "Metamaterials and negative refractive index," Science **305**(5685), 788–792 (2004).
11. H.-T. Chen, J. F. O'Hara, A. K. Azad, A. J. Taylor, R. D. Averitt, D. B. Shrekenhamer, and W. J. Padilla, "Experimental demonstration of frequency-agile terahertz metamaterials," Nat. Photonics **2**(5), 295–298 (2008).
12. H.-T. Chen, J. F. O'Hara, A. J. Taylor, R. D. Averitt, C. Highstrete, M. Lee, and W. J. Padilla, "Complementary planar terahertz metamaterials," Opt. Express **15**(3), 1084–1095 (2007).
13. J.-W. Dong, H. H. Zheng, Y. Lai, H.-Z. Wang, and C. Chan, "Metamaterial slab as a lens, a cloak, or an intermediate," Phys. Rev. B **83**(11), 115124 (2011).
14. G. Dolling, M. Wegener, C. M. Soukoulis, and S. Linden, "Negative-index metamaterial at 780 nm wavelength," Opt. Lett. **32**(1), 53–55 (2007).
15. H. O. Moser, B. D. Casse, O. Wilhelmi, and B. T. Saw, "Terahertz response of a microfabricated rod-split-ring-resonator electromagnetic metamaterial," Phys. Rev. Lett. **94**(6), 063901 (2005).
16. S. Zhang, Y.-S. Park, J. Li, X. Lu, W. Zhang, and X. Zhang, "Negative refractive index in chiral metamaterials," Phys. Rev. Lett. **102**(2), 023901 (2009).
17. T. Hofmann, U. Schade, C. Herzinger, P. Esquinazi, and M. Schubert, "Terahertz magneto-optic generalized ellipsometry using synchrotron and blackbody radiation," Rev. Sci. Instrum. **77**(6), 063902 (2006).
18. M. Brucherseifer, M. Nagel, P. H. Bolivar, H. Kurz, A. Bosserhoff, and R. Büttner, "Label-free probing of the binding state of DNA by time-domain terahertz sensing," Appl. Phys. Lett. **77**(24), 4049–4051 (2000).

#216710 - $15.00 USD Received 9 Jul 2014; revised 25 Aug 2014; accepted 2 Oct 2014; published 6 Nov 2014

19. P. Bolivar, M. Brucherseifer, M. Nagel, H. Kurz, A. Bosserhoff, and R. Büttner, "Label-free probing of genes by time-domain terahertz sensing," Phys. Med. Biol. **47**(21), 3815–3821 (2002).
20. X. Wang, Y. Cui, W. Sun, J. Ye, and Y. Zhang, "Terahertz polarization real-time imaging based on balanced electro-optic detection," J. Opt. Soc. Am. A **27**(11), 2387–2393 (2010).
21. H. Chen, H. Bian, J. Li, X. Guo, X. Wen, and J. Zheng, "Molecular Conformations of Crystalline l-Cysteine Determined with Vibrational Cross Angle Measurements," J. Phys. Chem. B **117**(49), 15614–15624 (2013).
22. P. Yeh, "A new optical model for wire grid polarizers," Opt. Commun. **26**(3), 289–292 (1978).
23. B. Scherger, M. Scheller, N. Vieweg, S. T. Cundiff, and M. Koch, "Paper terahertz wave plates," Opt. Express **19**(25), 24884–24889 (2011).
24. C.-Y. Chen, T.-R. Tsai, C.-L. Pan, and R.-P. Pan, "Room temperature terahertz phase shifter based on magnetically controlled birefringence in liquid crystals," Appl. Phys. Lett. **83**(22), 4497–4499 (2003).
25. M. Mazur and W. Zieniutycz, "Multi-layer meander line polarizer for Ku band," in *Microwaves, Radar and Wireless Communications. 2000. MIKON-2000. 13th International Conference on*, (IEEE, 2000), 78–81.
26. R. Singh, E. Plum, W. Zhang, and N. I. Zheludev, "Highly tunable optical activity in planar achiral terahertz metamaterials," Opt. Express **18**(13), 13425–13430 (2010).
27. R. Singh, E. Plum, C. Menzel, C. Rockstuhl, A. Azad, R. Cheville, F. Lederer, W. Zhang, and N. Zheludev, "Terahertz metamaterial with asymmetric transmission," Phys. Rev. B **80**(15), 153104 (2009).
28. A. C. Strikwerda, K. Fan, H. Tao, D. V. Pilon, X. Zhang, and R. D. Averitt, "Comparison of birefringent electric split-ring resonator and meanderline structures as quarter-wave plates at terahertz frequencies," Opt. Express **17**(1), 136–149 (2009).
29. F. Fang and Y. Cheng, "Dual-Band Terahertz Chiral Metamaterial with Giant Optical Activity and Negative Refractive Index Based on Cross-Wire Strucure," Prog. Electromag. Res. M **31**, 59–69 (2013).
30. J. Zhou, D. R. Chowdhury, R. Zhao, A. K. Azad, H.-T. Chen, C. M. Soukoulis, A. J. Taylor, and J. F. O'Hara, "Terahertz chiral metamaterials with giant and dynamically tunable optical activity," Phys. Rev. B **86**(3), 035448 (2012).
31. D. Zarifi, M. Soleimani, and V. Nayyeri, "A novel dual-band chiral metamaterial structure with giant optical activity and negative refractive index," J. Electromagn. Waves Appl. **26**(2-3), 251–263 (2012).
32. X. Ma, C. Huang, M. Pu, C. Hu, Q. Feng, and X. Luo, "Multi-band circular polarizer using planar spiral metamaterial structure," Opt. Express **20**(14), 16050–16058 (2012).
33. N. Kanda, K. Konishi, and M. Kuwata-Gonokami, "Terahertz wave polarization rotation with double layered metal grating of complimentary chiral patterns," Opt. Express **15**(18), 11117–11125 (2007).
34. C. Huang, X. Ma, M. Pu, G. Yi, Y. Wang, and X. Luo, "Dual-band 90° polarization rotator using twisted split ring resonators array," Opt. Commun. **291**, 345–348 (2013).
35. A. Ishikawa and T. Tanaka, "Plasmon hybridization in graphene metamaterials," Appl. Phys. Lett. **102**(25), 253110 (2013).
36. J. Hao, Y. Yuan, L. Ran, T. Jiang, J. A. Kong, C. T. Chan, and L. Zhou, "Manipulating electromagnetic wave polarizations by anisotropic metamaterials," Phys. Rev. Lett. **99**(6), 063908 (2007).

1. Introduction

Terahertz (THz) radiation has gained wide applications in the fields of spectroscopy [1–5], sensing and imaging [6–9]. In THz applications, one major difficulty is that most natural materials exhibit weak response to THz waves, so conventional optical elements such as waveplates, prisms and filters are difficult to find their counterparts in THz. The emergency of metamaterials [10–14], i.e. artificial electromagnetic materials which exhibit extraordinary responses in various desired frequency regimes, has enabled the manipulation of THz waves [15, 16] with their fascinating novel properties. However, for many practical applications this approach needs further explorations to fully exploit the attractive potential applications of THz waves.

Polarization, an important physical property of light wave, is critical in many applications. The polarization of a THz wave is of great importance in THz sensing and spectroscopy. For examples, the THz magneto-optic ellipsometry in the detection of Hall effect [17], sensing the chiral structures of proteins and DNA [18, 19], the THz polarization imaging [20] and the determination of 3D molecular structures [21] require effective THz polarization control devices.

Up to date, the most common polarizer in THz is the wire-grid polarizer [22]. Some commercially unavailable concepts like birefringence utilizing paper [23], liquid crystals [24], multi-layer meander liners [25] can also change THz polarization based on Faraday, Kerr, birefringence effects, etc. However, as mentioned in the first paragraph, the choice of THz responsible materials is limited, so the development of THz polarizing optical elements is far

#216710 - $15.00 USD Received 9 Jul 2014; revised 25 Aug 2014; accepted 2 Oct 2014; published 6 Nov 2014

inferior to its counterpart in the optical/infrared regime. By applying the concept of metamaterials, the polarization of THz wave can be flexibly controlled, e.g. the chiral effect by metamaterials [26–30] can be used to manipulate the polarization state of THz wave. For example, the asymmetric transmission of left and right circular-polarized wave can be realized [27]. A linear-to-circular polarization conversion in the range of 0.62-0.65 THz is realized by metamaterial [28]. The dual-band [31] and multi-band [32] circular polarizers are also demonstrated with the metamaterial concept. The THz wave linear polarization rotation on a single frequency based on the complimentary chiral pattern [33] and a dual-frequency [34] by two-layered twisted split ring resonators are also demonstrated. However, the bandwidth to center frequency ratio (BCR) are below 10% for the existing devices [28–34]. A broadband polarization convertor is yet to be realized in the THz frequency regime.

In this letter we theoretically design and experimentally demonstrate a broadband polarization rotator in the THz domain. This metamaterials-based THz polarization rotator can effectively rotate the polarization of reflected waves between 0.44 and 0.76 THz (more than 50% of the BCR) by 90 degree and exhibit nearly unity conversion efficiency. The device is a planar metamaterial containing three layers along the wave propagation direction.

2. Results and discussions

2.1 Device design

The designed device in this study is illustrated in Fig. 1(a) and 1(b). It consists of three layers of planar structures: (1) on the top is a two-dimensional array of tilted coupled split rings (TCSRs) made of gold of which the unit cell is illustrated in Fig. 1(b). The array has a periodicity of 150μm in the two orthogonal directions. The gold rings are 200nm thick on the top of 10nm Cr adhesive layer. The radii of the two rings r_1, r_2 are 40.5μm and 52.5μm respectively. The width w of the rings is 7.5μm, and the broken gap widths g of both rings are 4.5μm. The outer split ring is tilted by 45 degree clockwise and the inner one is tilted by 135 degree counter clockwise (the y-axis is 12 o'clock). (2) Underneath is a layer of polyimide with a thickness t of 50μm, and (3) the bottom layer is a flat gold surface. X-polarized THz wave is normal incident along the z-axis onto the metamaterial surface and reflected in the same direction. The polarization of the reflected wave changes for 90° to be along the y-axis.

2.2 Methods and materials

The fabrication of device contains several steps: (1) A Cr/Au layer with thickness of 10/200 nm was e-beam evaporated onto a flat silicon substrate in a UHV-chamber; (2) a 50-μm thick layer of polyimide (PI-2525, from HD microsystems, use as received) was spin-coated onto the Au surface and baked at 300 ^{o} C for 3 hours and cooled down to room temperature under ambient condition; (3) the TCSR array was fabricated directly onto the polyimide layer via the standard photolithographic technique: photoresist SU-1813 was spin coated onto the polyimide surface and exposed with a pre-made photo mask (by Frontrange Inc.). After development with MF-319 developer, a layer of Cr/Au with thickness of 10/200 nm was e-beam evaporated on the photoresist in an UHV-chamber. The standard lift-off process was then done with acetone spraying to remove the photoresist. One optical microscope image of the fabricated device is shown in Fig. 1(c). The preparation procedure is general and can be accessible in most clean rooms. Other methods, e.g. focus ion beam writing, laser direct writing and e-beam lithography can also be used to fabricate the top patterned layer, but the one we used is probably among the most economical and effective methods.

#216710 - $15.00 USD Received 9 Jul 2014; revised 25 Aug 2014; accepted 2 Oct 2014; published 6 Nov 2014

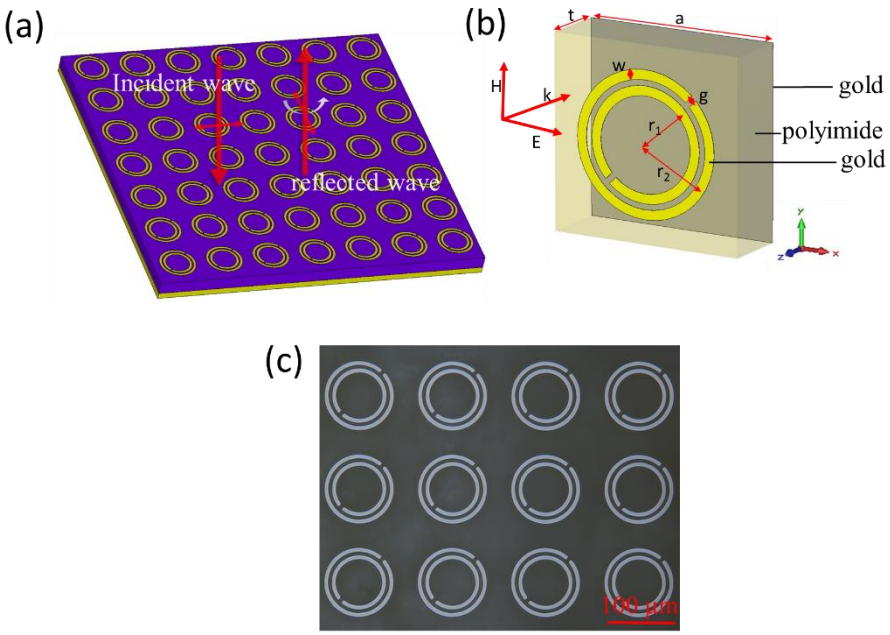

Fig. 1. Sketch of the metamaterial design, (a) illustration of TCSRs array and incident/reflected THz waves - an x-polarized THz wave incident to the metamaterial that is reflected as y-polarized. (b) Unit cell of the TCSRs, it contains three layers of materials as labeled. All dimensions are marked. (c) Optical microscope image of a fabricated sample. The brighter parts (split rings) are made of gold, and the darker parts are the polyimide layer on a gold plate.

Room-temperature THz reflection measurements were conducted with a THz time domain spectroscopy (TDS) setup illustrated in Fig. 2(a). A Ti/Sapphire laser produces 45 fs pulses at 780 nm with a repetition rate of 80 MHz that impinge onto an interdigitated switch at an average power of 725 mW. The switch is biased at 15 V with 50% duty cycle at 15.5 kHz and produces the THz pulse that first travels to the first wire-grid polarizer then a parabolic mirror and a Silicon beam splitter then onto a parabolic mirror finally to the sample surface. The reflected beam from the sample surface is reflected by the parabolic mirror, Silicon beam splitter and the second wire-grid polarizer then onto another parabolic mirror, and combines with the delayed 800nm probe beam. The combined beams are electro-optic sampled using a ZnTe crystal. The setup has a maximum beam waist on the sample surface of about 5 mm and a frequency resolution of 0.08 THz.

The extinction ratio of the polarizer pair is 27 dB. The polarization measurements are sketched in Fig. 2(b). To solve the issue that the detector only detects one polarization, we set both x- and y-polarizations 45 ^{o} relative to the polarization of detection by using two polarizers. First, the reference spectrum is obtained with a gold mirror (b1 in Fig. 2(b)). A control measurement to show that there is no depolarization in the optical path is also conducted by setting the 2nd polarizer 90 ^{o} to the first polarizer. Second, as shown in Fig. 2(b), the Co-polarization reflectance R_{xx} is measured with the sample replacing the gold mirror and with the two polarizers parallel to each other. Third, as shown in b3, the Cross-polarization reflectance R_{xy} is measured with the sample replacing the gold mirror and with the two polarizers perpendicular to each other. The x axis of the sample is along the first polarizer, as shown in b2 and b3. All measurements were in a dry air-purged environment in which the humidity is below 1% to avoid the influence of water vapor absorption. Reflection spectra are normalized to a gold mirror at the same position which functions as a reference object.

#216710 - $15.00 USD Received 9 Jul 2014; revised 25 Aug 2014; accepted 2 Oct 2014; published 6 Nov 2014

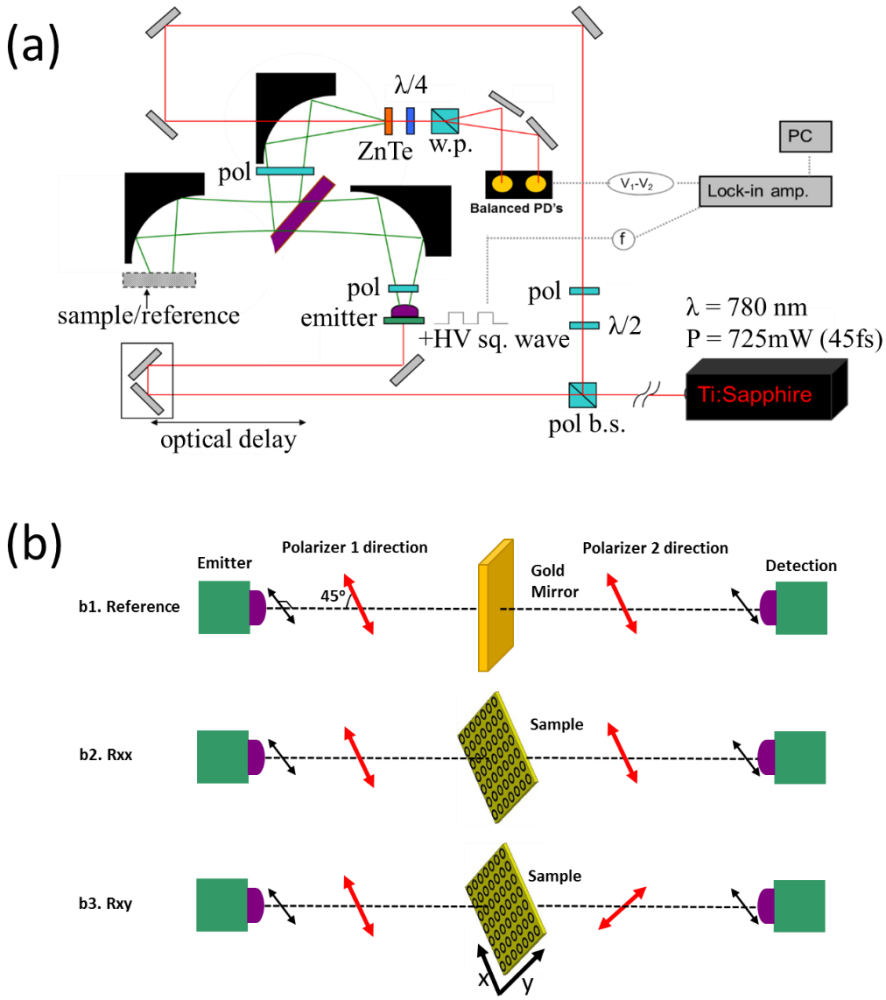

Fig. 2. (a) Optical setup of reflection measurement illustration. The red line represents the 780 nm laser, and the green lines are the traces of THz wave (b) sketch of measurements and polarizer angles. b1 is the reference measurement, b2 is for R_{xx} measurement and b3 is for R_{xy} measurement. Red arrows represent the polarizer directions. The x-axis of the sample is aligned to be along the first polarization direction.

To quantitatively understand the polarization rotation of the device, we performed full wave three dimensional numerical calculations with frequency domain finite integration methods using widely recognized metamaterial simulating commercial software CST MWS 2012. Bloch boundary conditions were applied in the two orthogonal (X-Y) directions. In the calculations, the absorbing boundary was used at the –Z and + Z directions to avoid S parameters errors by the reflection wave from the boundary. Gold is modeled as a Drude metal with a plasma frequency of 1.37×10^{16} rad/s and a collision frequency of 6.51×10^{12}/s. The permittivity of polyimide is taken to be 3.0.

2.3 Results and discussion

Here we define the incident polarization direction as x, the direction perpendicular to it within the device surface plane as y, and the THz wave incident direction as z. The perpendicular reflectance $R_{xy} = E_{yr} / E_{xi}$ is the ratio of reflected (r) electric field along the y direction (E_{yr})

#216710 - $15.00 USD Received 9 Jul 2014; revised 25 Aug 2014; accepted 2 Oct 2014; published 6 Nov 2014

over the incident (i) electric field that is along the x direction (E_{xi}), and the parallel reflectance $R_{xx} = E_{xr} / E_{xi}$ is the ratio of reflected electric field along the x direction (E_{xr}) over the incident electric field along the same direction (E_{xi}).

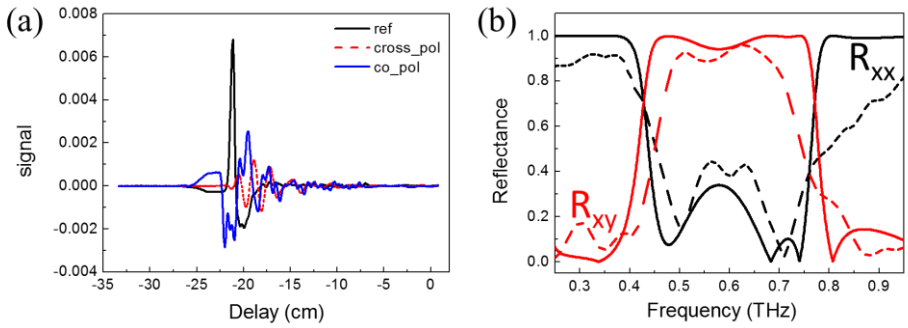

Fig. 3. (a) Time domain THZ signal. The black curve is from the reference object, the blue curve is from the co-polarization measurement, and the dash red curve is from the cross-polarization measurement. (b) Calculated (solid) and measured (dash) reflectance spectra from the normal incident direction. R_{xx} (black) is the parallel reflectance and R_{xy} (red) is the perpendicular reflectance.

Figure 3(a) shows the time-domain data from measurements on reference, cross- and co-polarization of the sample. After Fourier transformation, we retrieve the frequency domain reflectance. The dash lines in Fig. 3(b) displays the measured reflectance with polarization perpendicular (red) to that of the normal incident broadband THz light and the reflectance with the same polarization (black) as that of the incident light reflected from the device. As we can see from Fig. 3(b), the polarization of more than 90% of the incident electric field (R_{xy} , red) (>80% of the incident photons) from ~0.48 THz to ~0.72 THz rotates from x to y after reflected from the device, and only about an average of 20% (lowest 1% and highest 40%) of the electric field (R_{xx} , black) (4% of the incident photons) within the operational frequency range remains the incident polarization after reflection. The results demonstrate that a THz polarization rotator in a relatively broad frequency range is experimentally realized.

The experimental results are in very good agreements with theoretical calculations (the solid curves). The solid lines in Fig. 3(b) are the calculated reflectances R_{xx} and R_{xy} . The calculations show that within the frequency range of 0.44 to 0.76 THz, R_{xy} is nearly unity and R_{xx} is very small, indicating that a broadband polarization rotation for almost 90 ^{o} can be realized in the designed metamaterial device, of which the bandwidth to central frequency ratio exceeds 50%. The calculations confirm that the broadband polarization rotation is from the designed planar metamaterial structure. Careful examinations also find that the experimental bandwidth is slightly narrower than the calculated value and the experimental polarization conversion ratios are slightly lower than the calculations. We attribute such minor differences to the imperfection of experimental conditions, e.g. the absorption from residue photoresist and dielectric layer, defects of TCSRs, the non-uniform and errors in thickness of dielectric layer, and the non-uniformness of TCSRs over large area.

#216710 - $15.00 USD Received 9 Jul 2014; revised 25 Aug 2014; accepted 2 Oct 2014; published 6 Nov 2014

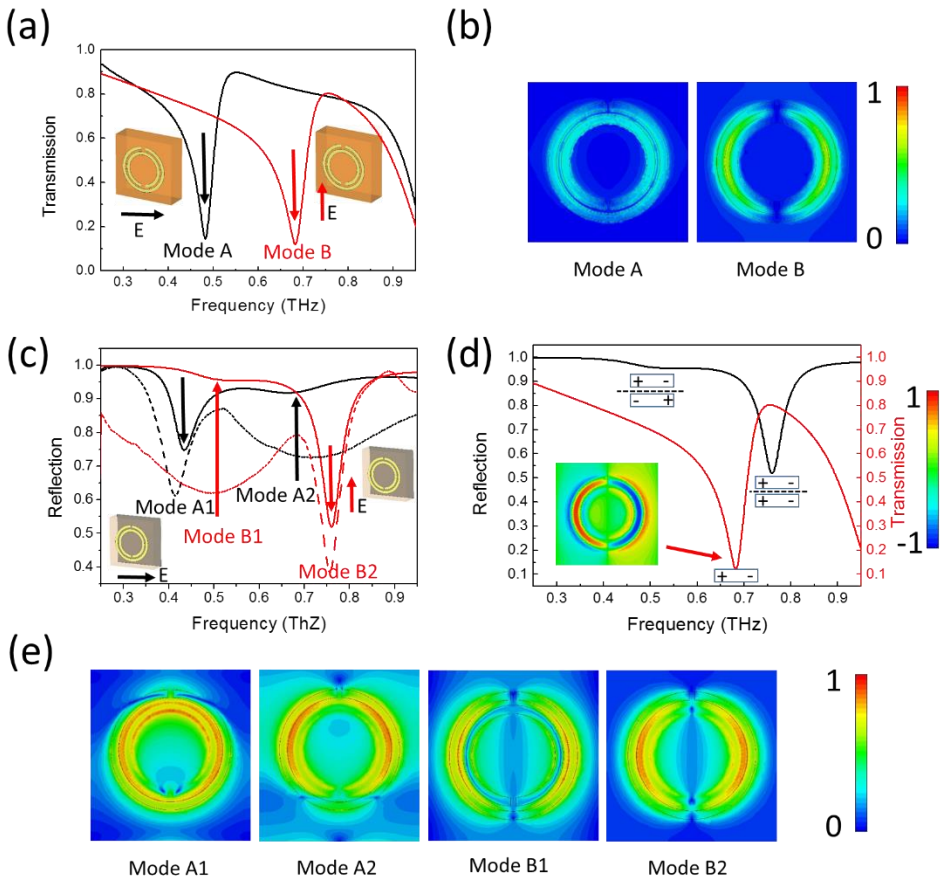

Fig. 4. Calculation and experimental results for the non-tilted coupled rings: (a) Transmission spectra without the back mirror. Black and red lines represent the x and y polarization, respectively. (b) Magnetic field distributions |H| of mode A and mode B. (c) Reflectance spectra with the back mirror. Positions of modes are marked with arrows. Solid lines are simulation results and dash lines show the experimental results: red (y-polarization) and black (x-polarization). (d) Illustration of plasmon hybridization of mode B splitting into modes B1 and B2. (e) Electric field distributions of modes A1, A2, B1, and B2.

To understand how the designed structure realizes the functions, we first study the plasmonic modes in non-tilted TCSR structures which cannot change the polarization to illustrate the principle of realizing the relatively broad bandwidth. The calculated transmission spectra for a non-tilted couple-rings structure (the two broken gaps are along the y-direction in opposite sides) without a back gold mirror are plotted in Fig. 4(a). In the spectra, there are two peaks at about 0.48 THz and 0.68 THz respectively. The peak at the lower frequency named as mode A can only be excited by the x-polarized light. The higher frequency peak named mode B can only be excited by the y-polarized light. The modulus of H field distributions of both modes are displayed in Fig. 4(b), showing that mode A is a magnetic-like plasmonic mode while mode B is electric-like. When the gold back mirror is inserted onto the other side of polyimide, two peaks show up in each polarization-dependent reflectance spectrum as displayed by the solid lines in Fig. 4(c). As we can see from Fig. 4(c), the simulated and experimental spectra agree with each other reasonably well. The generation of two peaks in each polarization is because of the plasmon hybridization [35] from the top rings and their mirror images produced from the back reflector (mirror), as depicted in Fig. 4(d). In Fig. 4(d), the red curve is the transmission spectrum without the back mirror. The

#216710 - $15.00 USD Received 9 Jul 2014; revised 25 Aug 2014; accepted 2 Oct 2014; published 6 Nov 2014

phase of field distribution of mode B is plotted in the inset. The black curve is the reflection spectrum with the back mirror. The blocks with symbols "+" and "-" in the figure represent the phases of the modes. When a back reflector is introduced, two different phases of the mirror images are created at two different frequencies: co-phased and anti-phased (to the plasmon modes). Mode B (0.68 THz) splits into two modes B1 (0.52 THz, anti-phased and therefore it is small) and B2 (0.76 THz, co-phased and therefore it is big). In a similar manner, mode A splits into modes A1 and A2. The moduli of magnetic field distributions |H| of four modes are shown in Fig. 4(e). As discussed, because of the mode hybridization, two frequencies rather than a single frequency are reflected by the TCSR structures with a back reflector for each polarization direction.

The mode hybridization is critical for the broadband polarization rotation of the **tilted** structure. When the x-polarized THz wave within 0.44 to 0.76 THz is incident normally onto the **tilted** metamaterials (Fig. 1(a)), its component perpendicular to the connection line of the two slits of the rings excites modes A1, A2, and the component along the connection line excites modes B1, B2. However, these four modes are not independent. They interact with each other, and the reflected spectra (Fig. 3(a)) are determined by such an interaction which is affected by almost all parameters of the whole device structure including the thickness of the polyimide dielectric spacing. From calculations, we found that 50μm is the optimum thickness for the polyimide layer in order for our device to realize the nearly unity polarization rotation over a broad frequency range.

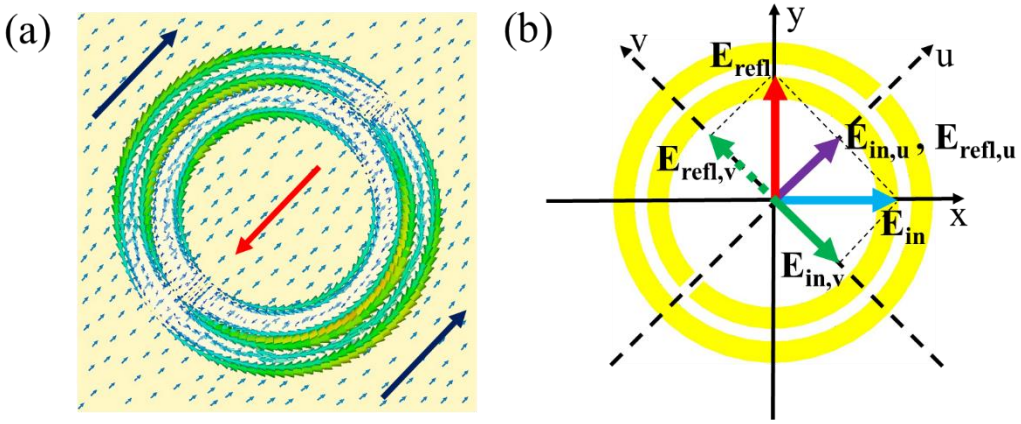

Fig. 5. Surface current distribution and illustration of polarization conversion. (a) Surface current distribution at 0.44 THz. The arrows around the rings are the simulated surface current distribution on the tilted couple rings layer. The total current direction is represented by the red arrow. The arrows on the light yellow plane are the surface current distribution on the back reflector. The total current direction is represented by the deep blue arrows. (b) Illustration to show a polarization rotation. The light blue arrow is the incident x-polarized THz wave. Its v component is the solid green arrow. Its u component is the violet arrow. The reflected wave is the red arrow. The reflected v component is the dash green arrow as it is 180 degree out of phase from the incident component, and the u component is also the violet arrow because the reflection is in phase in this direction.

Furthermore, we investigate how the polarization rotation occurs. Figure 5(a) is the simulated surface current distributions of the top tilted coupled rings and the back reflector layer at 0.44 THz. As we can see, the direction of the current on the rings (red arrow) is opposite to that on the back reflector surface (deep blue arrows). Such surface current distributions form a magnetic resonance [36], which means that the permeability tensor component along the u axis (Fig. 5(b)) of the metamaterial becomes very large. Therefore, the material behaves like a high-impedance surface along the u axis, leading to the in-phase reflection in this direction (the u component of the reflected wave is along its original

#216710 - $15.00 USD Received 9 Jul 2014; revised 25 Aug 2014; accepted 2 Oct 2014; published 6 Nov 2014

direction), as shown in Fig. 5(b). Along the v axis the permeability tensor is small [36], and the incident wave "sees" the back mirror and is reflected with a phase change of 180 degree (the dash green in Fig. 5(b)). Because there is almost no loss during reflection (ideally), the sum of the reflected components along both axes produces a polarization along the y-axis. In other words, the incident polarization along x-axis has been rotated for 90 degree to be along with the y-axis after the reflection because of the different phase shifts of the reflected components long the u and v axes.

3. Conclusion

We demonstrate a planar metamaterial THz broadband polarization convertor which rotates the normal incident linearly polarized wave into its orthogonal polarization. THz-TDS reflection measurements were conducted to prove the effectiveness of the device and full wave simulations were applied to verify and explain the working principle in theory. The ideal bandwidth to central frequency ratio of the device exceeds 50%. The design can be scalable to fit any desired frequency range, and it can be easily designed into active-controlled devices when optical or electrical controls are introduced. We expect such metamaterial devices to have potential in THz imaging and polarimetry applications.

Acknowledgments

This material is based upon work supported by AFOSR Award No. FA9550-11-1-0070, and the Welch foundation under Award No. C-1752. J. R. Zheng also thanks the David and Lucile Packard Foundation for a Packard fellowship and the Alfred P. Sloan Foundation for a Sloan fellowship. X.W. thanks D. Nickel and Dr. D. Mittleman for great help and discussion in experiments.